

Altermagnetic Spin-Splitting Magnetoresistance

Hongyu Chen^{1,4}, Zian Wang^{2,3,4}, Peixin Qin^{1*}, Ziang Meng¹, Xiaorong Zhou¹, Xiaoning Wang¹, Li Liu¹, Guojian Zhao¹, Zhiyuan Duan¹, Tianli Zhang¹, Jinghua Liu^{1*}, Dingfu Shao^{2,3*}, and Zhiqi Liu^{1*}

¹School of Materials Science and Engineering, Beihang University; Beijing 100191, China.

²Key Laboratory of Materials Physics, Institute of Solid State Physics, HFIPS, Chinese Academy of Sciences; Hefei 230031, China.

³Science Island Branch of Graduate School, University of Science and Technology of China; Hefei 230026, China.

⁴These authors contributed equally: Hongyu Chen, Zian Wang

*e-mail: qinpeixin@buaa.edu.cn; 09077@buaa.edu.cn; dfshao@issp.ac.cn;
zhiqi@buaa.edu.cn

Abstract

The recently discovered altermagnets, featured by the exotic correlation of magnetic exchange interaction and alternating crystal environments, have offered exciting cutting-edge opportunities for spintronics. Here, we report the experimental observation of an altermagnetic spin-splitting magnetoresistance effect, which is driven by a spin current associated with the giant nonrelativistic spin splitting of an altermagnet. The spin current polarization and the corresponding magnetic field direction associated with the magnetoresistance extrema are largely determined by the Néel vector of the altermagnet, leading to a remarkable phase shift compared to that driven by a conventional relativistic spin current. Our work opens a door to unearthing luxuriant nonrelativistic quantum states of matter in emergent materials with unconventional spin degeneracy lifting.

Recent theoretical and experimental studies on some unconventional antiferromagnets have unveiled an exotic magnetic phase dubbed altermagnetism [1–3]. Distinct from ferromagnets and conventional antiferromagnets, altermagnets are typically composed of two opposite magnetic sublattices that are connected by crystal rotation symmetries. Such alternating magnetic structures break the time-reversal (\mathcal{T}) symmetry, thus engendering sizable spin splitting with alternating spin polarization in momentum space in the absence of relativistic spin-orbit coupling (SOC) (refs. [1–3]). Consequently, altermagnets are endowed with various \mathcal{T} -symmetry-breaking responses and spin-polarization-related phenomena that are ubiquitous in ferromagnets and constitute the bases of ferromagnetic spintronics, such as the anomalous Hall effect [4–7], x-ray magnetic circular dichroism [8,9], giant/tunneling magnetoresistance [10–12], and spin transfer torques [12], despite their vanishing net magnetic moment.

Among these exotic properties, the altermagnetic spin-splitting effect (SSE) has received a surge of interest recently [13–17]. Taking RuO_2 [Fig. 1(a)], a prototypical altermagnet candidate as an example [1,2], an electric field applied along [010] can generate a net nonrelativistic spin current along [100] as a result of the anisotropy of the spin-split electronic bands, as illustrated in Fig. 1(b). Remarkably, since the spin polarization in momentum space is parallel to the Néel vector in real space, the engendered spin current is highly tunable [13]. For instance, via rotating RuO_2 around its [010] crystal axis to obtain a (101)-oriented thin film, an out-of-plane spin current with tilted spin polarization can be induced by an electric field along [010] [Fig. 1(c)]

(refs. [14,16,17]). Such spin currents with an unconventional polarization direction can lead to the field-free switching of an adjacent ferromagnetic layer with perpendicular magnetic anisotropy [16]. Moreover, the reciprocal process of the SSE—the inverse spin-splitting effect (ISSE)—has also been demonstrated, wherein the anisotropic spin-split electronic bands convert spin currents with spin polarization parallel to the Néel vector into charge currents [17,18].

Here we experimentally show that the SSE/ISSE can lead to a new nonrelativistic magnetoresistance effect, which we dub the altermagnetic spin-splitting magnetoresistance (SSMR), in an altermagnet/ferromagnet bilayer of (101)-RuO₂/Co. We notice that the altermagnetism of bulk RuO₂ are currently under intense debate [19–23]. On the other hand, recent theoretical and experimental studies have indicated long-range magnetic order in ultrathin RuO₂ films with epitaxial strain and (or) point defects [22,24–27], which is well consistent with our results.

Sketch of the altermagnetic spin-splitting magnetoresistance—We start with a sketch of the SSMR. As depicted in Fig. 1(c), in a (101)-oriented RuO₂ thin film, an electric field \mathbf{E} along [010] generates an out-of-plane spin current \mathbf{J}^p with spin polarization \mathbf{p} . In the absence of SOC, \mathbf{J}^p is solely engendered by the SSE and thus \mathbf{p} is parallel to the Néel vector \mathbf{n} (along [001]) of RuO₂. Then \mathbf{J}^p is reflected by the RuO₂/Co interface, with the reflection strength modulated by the relative orientation between \mathbf{p} and the magnetization direction \mathbf{m} of Co. When \mathbf{p} is perpendicular (parallel) to \mathbf{m} , the reflection is minimized (maximized) due to the strong (weak) absorption of \mathbf{J}^p by Co. The

reflected spin current is converted to an additional longitudinal charge current J_r^c via the ISSE, lowering the longitudinal resistance of the heterostructure, *i.e.*, a magnetoresistance effect. Consequently, when rotating \mathbf{m} in a plane perpendicular to \mathbf{E} by an angle β , the longitudinal resistance minimizes at $\beta = \beta_0$ wherein \mathbf{m} is parallel to \mathbf{p} . In the absence of SOC, β_0 is exactly the out-of-plane tilting angle $\theta_n \sim 34^\circ$ of the \mathbf{n} in (101)-RuO₂.

The underlying physics of the SSMR can be compared with that of the celebrated spin Hall magnetoresistance (SMR) in nonmagnet/ferromagnet heterostructures [28–30]: (1) Both effects are underpinned by the modification of the charge-spin interconversion processes in the nonmagnetic layer by \mathbf{m} . (2) The SMR stems from the relativistic-SOC-induced (inverse) spin Hall effect and (or) the (inverse) Rashba-Edelstein effect while the SSMR is of a nonrelativistic origin and is thus in principle more prominent in magnitude. On the other hand, the phenomenology of the SSMR is distinct from the conventional SMR in high-symmetry systems. Taking (101)-RuO₂/Co as an example: (1) For \mathbf{E} applied along [010], the β -dependent magnetoresistance minimizes at $\beta_0 \sim 90^\circ$ in the SMR whereas it minimizes at $\beta_0 = \theta_n$ in the SSMR. We notice that the low symmetry of RuO₂ (101) can also lead to a slight tilt of \mathbf{p} toward the out-of-plane direction [14]. However, the tilt is negligible as shown in the subsequent sections of this article so that (101)-RuO₂/Co can be treated as a system yielding conventional SMR. (2) When changing the direction of the in-plane \mathbf{E} , β_0 almost remains a constant of 90° in the SMR, but it significantly varies in the SSMR as imposed by the interfacial

reflection strength of \mathcal{J}^p and the anisotropy of the (I)SSE. Therefore, the SSMR can serve as a simple electric probe for characterizing \mathbf{n} and the anisotropic spin-split Fermi surfaces of altermagnets.

It should be mentioned that the β -dependent magnetoresistance of (101)-RuO₂/Co in our study inevitably comprises notable contributions from the SMR apart from the SSMR due to the strong SOC of Ru (refs. [14,31,32]). As a result, the β_0 deviates from θ_n for \mathbf{E} applied along [010]. Nevertheless, through detailed temperature- and current-direction-dependent measurements as well as first principles calculations, we can unambiguously demonstrate the existence of the SSMR.

Spin-splitting magnetoresistance in a (101)-RuO₂/Co bilayer—The (101)-RuO₂ epilayers in this study were grown on (101)-TiO₂ substrates utilizing the pulsed laser deposition technique following a recipe developed in our previous work [5]. The x-ray diffraction pattern of a 22-nm-thick sample indicates that the RuO₂ thin film is (101)-oriented with high crystallinity and a smooth surface (Fig. S1, Supplemental Material [33]). After cooling down to room temperature, a thin Co layer of ~2.5 nm was deposited on top of RuO₂ through magnetron sputtering. In order to prevent the Co from oxidization, all the samples are capped with a sputtered 2-nm-thick Al layer. The thin films were subsequently patterned into Hall bars with a channel width W of ~3 μm and a separation between two longitudinal voltage probes $L \sim 5W$ to study the magnetotransport properties, as depicted in Fig. 2(a).

We first focus on the angular-dependent magnetoresistance of a RuO₂(3 nm)/Co(2.5 nm) bilayer. The definitions of the coordinate system and the rotation angles of the applied magnetic field (α , β , and γ) are illustrated in Fig. 2(b). The current is applied along the x axis and the applied field is 3 T in our study unless otherwise specified. As depicted in Fig. 2(c), the R_{xx} measured along [010] reaches a minimum at $\beta_0 \sim 55^\circ$ with $R_{xx}(\beta) \propto \sin^2(\beta - \beta_0)$ at 50 K, in sharp contrast to the conventional SMR wherein $\beta_0 \sim 90^\circ$ and $R_{xx}(\beta) \propto \cos^2\beta$ (refs. [28–30]). Such an anomaly is not induced by the angular offset in our measurement since the α - and γ -dependent R_{xx} with extrema occurring at 0° , 90° , $180^\circ \dots$ can be well interpreted by the anisotropic magnetoresistance (AMR) of Co [Fig. 2(d)]. In addition, the AMR of a (101)-RuO₂ thin film is negligible (Fig. S2, Supplemental Material [33]) so that it cannot lead to the prominent $R_{xx}(\beta)$. We also rule out the possible experimental artifact originating from the strong magnetic anisotropy of the Co layer in concert with insufficient measurement magnetic fields (Supplemental Note 2 [33]). Therefore, the anomalous $R_{xx}(\beta)$ is ascribed to the existence of the SSMR in the sample.

We define the difference between the maximum and the minimum value of $R_{xx}(\beta)$ as the (S)SMR $\Delta R_{xx}^{(S)SMR}$, as illustrated in Fig. 2(c) and detailed in Supplemental Note 1 [33]. Note that the $\Delta R_{xx}^{(S)SMR}$ of $\sim 0.17 \Omega$ cannot be extracted from conventional field-dependent magnetoresistance measurements (Fig. S5, Supplemental Material [33]), in contrast to the SMR (refs. [28–30]). As discussed in the previous part of this article, the $\Delta R_{xx}^{(S)SMR}$ contains contributions from both the SSMR and the SMR. This is further

supported by the fact that the $\beta_0 > \theta_n$, *i.e.*, the \mathbf{p} of the out-of-plane spin current in RuO₂ is tilted away from \mathbf{n} toward the y axis. For simplicity, we calculate the (S)SMR ratio as $\Delta R_{xx}^{(S)SMR}/R_{xx}(0)$, where $R_{xx}(0)$ is the longitudinal resistance of the heterostructure at $\beta = 0^\circ$. The deduced (S)SMR ratio is $\sim 9 \times 10^{-5}$ at 50 K, smaller than the typical SMR ratio for heavy metal/ferromagnet bilayers [28–30] despite the predicted large spin conductivity σ^p for the SSE of RuO₂ (ref. [13]). This can stem from the time-reversal-odd (\mathcal{T} -odd) nature of the SSE, *i.e.*, the σ^p from opposite magnetic domains compensates each other, leading to a small net σ^p .

In order to shed more light on the (S)SMR, we study the temperature dependence of the $R_{xx}(\beta)$ of the sample. It is found that the (S)SMR is robust against a temperature of at least 300 K (Fig. S6, Supplemental Material [33]). The β_0 deduced from measurements along [010] augments by $\sim 9^\circ$ and the (S)SMR ratio decreases by a factor of ~ 5.6 with temperature increased from 50 to 300 K (Fig. 3). As discussed in the previous section, the SSE generates spin currents with a well-defined \mathbf{p} that is parallel to \mathbf{n} . In addition, the (I)SSE can be strongly disturbed by temperature owing to their intimate correlation with altermagnetism and their sensitivity to electron scattering [13,14,17,18]. Therefore, the β_0 is expected to be independent of temperature while the $\Delta R_{xx}^{SSMR}/R_{xx}(0)$ is presumed to be diminished by increased temperature for the SSMR. On the other hand, the spin Hall effect and (or) the Rashba-Edelstein effect that are responsible for the SMR engender spin currents with \mathbf{p} close to the y axis, and typically they are relatively insensitive to temperature [45,46]. As a result, the shape of the $R_{xx}(\beta)$ curves and the

$\Delta R_{xx}^{\text{SMR}}/R_{xx}(0)$ are anticipated to yield much weaker dependence on temperature for the SMR (refs. [47,48]). Consequently, the remarkable variation of both the β_0 and the $\Delta R_{xx}^{(\text{S})\text{SMR}}/R_{xx}(0)$ with raised temperature in Fig. 3 unambiguously demonstrates the coexistence of the SSMR and the SMR in the sample. In particular, the gradual increase of β_0 from 50 to 300 K indicates that the \mathbf{p} becomes closer to the y axis at higher temperature, consistent with the weakness of the SSMR under stronger thermal disturbance.

We next investigate the β -dependent magnetoresistance measured along $[\bar{1}01]$ to highlight the existence of the SSMR. As can be deduced from Fig. 1(b), the SSE does not contribute to the out-of-plane spin current in a (101)-RuO₂ thin film for an \mathbf{E} applied along $[\bar{1}01]$ (refs. [13,14,17]). Therefore, the $R_{xx}(\beta)$ measured along $[\bar{1}01]$ is similar to that expected for a conventional SMR effect. As depicted in Fig. 3, the β_0 remains a constant of $\sim 90^\circ$ and the $\Delta R_{xx}^{\text{SMR}}/R_{xx}(0)$ decreases rather slowly with increased temperature. This is in sharp contrast to the situation wherein $R_{xx}(\beta)$ is measured along $[010]$, solidifying the existence of the SSMR since the conventional SMR is not expected to change for \mathbf{E} applied along different direction.

Robustness of the spin-splitting magnetoresistance—To demonstrate the robustness of the SSMR, the $R_{xx}(\beta)$ of a RuO₂(3 nm)/Cu(1 nm)/Co(2.5 nm) control sample is investigated, where the inserted Cu layer is expected to suppress the reflection of the \mathcal{T} -odd spin current associated with SSE. As shown in Fig. 4(a), the insertion of Cu significantly changes the $R_{xx}(\beta)$ curves at 50 K. We find in this case the AMR ($R_{xx} \propto$

$\sin^2\beta$) of Co [49] is dominant. However, anomalies can be still found for β_0 away from 90° , indicating that the existence of SSMR even for the strong suppression of spin current reflection.

We also study $R_{xx}(\beta)$ as a function of the RuO₂ thickness t to further confirm the ubiquity of the SSMR. Notably, all the examined samples exhibit a $\beta_0 < 90^\circ$, demonstrating the universal existence of the SSMR in (101)-RuO₂(t)/Co(2.5 nm) with t of at least 10 nm. In addition, the augmentation of β_0 from $\sim 45^\circ$ at $t = 1$ nm to $\sim 75^\circ$ at $t = 10$ nm at 50 K [Fig. 4(b)] indicates that the SMR gradually prevails the SSMR with increased t . Furthermore, the $\Delta R_{xx}^{(S)SMR}/R_{xx}(0)$ is $\sim 9 \times 10^{-5}$ at $t = 1-3$ nm, but it rapidly decreases to $\sim 4 \times 10^{-6}$ at $t = 10$ nm [Fig. 4(c)]. We suggest that these features could result from the pronounced multidomain nature and (or) the loss of altermagnetism in thick samples, which deteriorates the (I)SSE and thus the SSMR. This also implies that interfacial strain could be indispensable for the stabilization of altermagnetism in RuO₂.

Theoretical considerations—The above observations are consistent with our theoretical analyses and first principles calculations. In a RuO₂ thin film, an \mathbf{E} generates an out-of-plane spin current \mathbf{J}^p as $\mathbf{J}^p = \boldsymbol{\sigma}^p \mathbf{E}$, where the spin conductivity $\boldsymbol{\sigma}^p = (\sigma^x, \sigma^y, \sigma^z)$ can be decomposed to the σ^x , σ^y , and σ^z components. On the other hand, the longitudinal charge current converted from the interface-reflected \mathbf{J}^p is $\mathbf{J}_r^c \propto (\boldsymbol{\sigma}^p \mathbf{m})^2$. Therefore, the R_{xx} minimizes at $\beta_0 = \cot^{-1}(\sigma^z/\sigma^y)$. (101)-RuO₂ hosts a glide mirror M_{010} perpendicular to [010] direction. When \mathbf{E} is applied along $[\bar{1}01]$ direction, only the conventional σ^y component is allowed due to \mathbf{E} being parallel to M_{010} [Fig. 5(a)]. This leads to $\beta_0 = \cot^{-1}$

$\theta(0) = 90^\circ$ as observed in Fig. 3(a). On the other hand, a [010] directional \mathbf{E} is perpendicular to M_{010} , allowing the unconventional σ^z in addition to σ^y [Fig. 5(b)]. Then $\beta_0 = \cot^{-1}(\sigma^z/\sigma^y) < 90^\circ$ is expected.

The spin conductivity σ^p of RuO₂ can be generated by the SSE (σ_{SSE}^p) and SHE (σ_{SHE}^p) from bulk RuO₂, and by the interfacial SOC (σ_{SOC}^p). Here we calculate the σ_{SSE}^p and σ_{SHE}^p based on linear response theory using first principles calculation. Since σ_{SSE}^p is associated with the Fermi surface, it is strongly influenced by scattering that depends on temperature. This is simulated by including an energy broadening Γ in the calculation. Using the typical Γ of 25 and 50 meV, we predict sizable $\sigma_{\text{SSE}}^p = (0, \sigma_{\text{SSE}}^y, \sigma_{\text{SSE}}^z)$ much larger than $\sigma_{\text{SHE}}^p = (0, \sigma_{\text{SHE}}^y, \sigma_{\text{SHE}}^z)$ when \mathbf{E} is along [010]. However, the β_0 of 38° (41°) is derived if we only consider σ_{SSE}^p and σ_{SHE}^p for Γ of 25 (50) meV (Supplemental Note 3 [33]). On the other hand, since the interfacial SOC is usually notable, we assume an additional $\sigma_{\text{SOC}}^y = 1000 (\Omega \text{ cm})^{-1}$, and obtain $\beta_0 = 52^\circ$ for $\Gamma = 25$ meV and 61° for $\Gamma = 50$ meV, as shown in Fig. 5(c). In the angular dependence of $(\sigma^p \mathbf{m})^2$ we define the difference between the maximum and minimum as $\Delta\Gamma$ [Fig. 5(c)], and find $\Delta(25 \text{ meV})/\Delta(50 \text{ meV}) = 2.3$, qualitatively consistent with the variation of (S)SMR ratio shown in Fig. 3(b). We thus believe that the observed $R_{xx}(\beta)$ is due to the cooperation of SSE of RuO₂ and the interfacial SOC.

Conclusions—In summary, we experimentally observe a new nonrelativistic magnetoresistance effect—the spin-splitting magnetoresistance. We unambiguously demonstrate the existence and the robustness of the SSMR in a (101)-RuO₂/Co bilayer.

The unique phenomenology of the SSMR makes it a simple electric probe for detecting the Néel vector orientation and characterizing the spin-split Fermi surface of altermagnets. We also note that due to the strong SOC of Ru, the SSMR is unavoidably contaminated by the SMR in our experiments. Nevertheless, the combined (S)SMR is still a powerful tool for revealing the reorientation of Néel vectors induced by spin torques and (or) magnetic fields without resort to complex magnetic tunnel junctions [50–52] or lock-in techniques [53,54]. Finally, we point out that the SSMR can also exist in other low-symmetry antiferromagnets with momentum-dependent spin splitting [55–60]. Therefore, our work opens an avenue to study the emerging materials with unconventional spin degeneracy lifting.

Acknowledgements—P.Q. acknowledges funding from National Natural Science Foundation of China (Grant No. 52401300). Z.L. acknowledges funding from National Natural Science Foundation of China (Grant No. 52425106). Z.L. and C.J. acknowledge funding from National Natural Science Foundation of China (Grant No. 52121001). Z.L. acknowledges funding from National Natural Science Foundation of China (Grant No. 52271235) and from National Key RandD Program of China (Grants Nos. 2022YFA1602700 and 2022YFB3506000). D.S. acknowledges funding from National Natural Science Foundation of China (Grants Nos. 12274411, 12241405, and 52250418), from Basic Research Program of the Chinese Academy of Sciences Based on Major Scientific Infrastructures (Grant No. JZHKYPT-2021-08), and from CAS

Project for Young Scientists in Basic Research (Grant No. YSBR-084). Z.L. acknowledges funding from Beijing Natural Science Foundation (Grant No. JQ23005). P.Q. acknowledges funding from China National Postdoctoral Program for Innovative Talents (Grant No. BX20230451) and from China Postdoctoral Science Foundation (Grant No. 2024M754058). D.S. acknowledges Hefei Advanced Computing Center. This work was also supported by the Academic Excellence Foundation for Ph.D. students of Beihang University. This work is also supported by “the Fundamental Research Funds for the Central Universities”.

References

- [1] L. Šmejkal, J. Sinova, and T. Jungwirth, Beyond conventional ferromagnetism and antiferromagnetism: A phase with nonrelativistic spin and crystal rotation symmetry. *Phys. Rev. X* **12**, 031042 (2022).
- [2] L. Šmejkal, J. Sinova, and T. Jungwirth, Emerging research landscape of altermagnetism. *Phys. Rev. X* **12**, 040501 (2022).
- [3] Krempaský, J. *et al.* Altermagnetic lifting of Kramers spin degeneracy. *Nature* **626**, 517–522 (2024).
- [4] L. Šmejkal, R. González-Hernández, T. Jungwirth, and J. Sinova, Crystal time-reversal symmetry breaking and spontaneous Hall effect in collinear antiferromagnets. *Sci. Adv.* **6**, eaaz8809 (2020).
- [5] Z. Feng, *et al.*, An anomalous Hall effect in altermagnetic ruthenium dioxide. *Nat. Electron.* **5**, 735–743 (2022).
- [6] R. D. Gonzalez Betancourt, *et al.*, Spontaneous anomalous Hall effect arising from an unconventional compensated magnetic phase in a semiconductor. *Phys. Rev. Lett.* **130**, 036702 (2023).
- [7] H. Reichlova, *et al.*, Observation of a spontaneous anomalous Hall response in the Mn_5Si_3 *d*-wave altermagnet candidate. *Nat. Commun.* **15**, 4961 (2024).
- [8] A. Hariki, *et al.*, X-ray magnetic circular dichroism in altermagnetic α -MnTe. *Phys. Rev. Lett.* **132**, 176701 (2024).
- [9] A. Hariki, Y. Takahashi, and J. Kuneš, X-ray magnetic circular dichroism in RuO_2 . *Phys. Rev. B* **109**, 094413 (2024).
- [10] D.-F. Shao, *et al.*, Néel spin currents in antiferromagnets. *Phys. Rev. Lett.* **130**, 216702 (2023).
- [11] L. Šmejkal, A. B. Hellenes, R. González-Hernández, J. Sinova, and T. Jungwirth, Giant and tunneling magnetoresistance in unconventional collinear antiferromagnets with nonrelativistic spin-momentum coupling. *Phys. Rev. X* **12**, 011028 (2022).

- [12] D.-F. Shao, S.-H. Zhang, M. Li, C.-B. Eom, and E. Y. Tsymbal, Spin-neutral currents for spintronics. *Nat. Commun.* **12**, 7061 (2021).
- [13] R. González-Hernández, *et al.*, Efficient electrical spin splitter based on nonrelativistic collinear antiferromagnetism. *Phys. Rev. Lett.* **126**, 127701 (2021).
- [14] A. Bose, *et al.*, Tilted spin current generated by the collinear antiferromagnet ruthenium dioxide. *Nat. Electron.* **5**, 267–274 (2022).
- [15] H. Bai, *et al.*, Observation of spin splitting torque in a collinear antiferromagnet RuO₂. *Phys. Rev. Lett.* **128**, 197202 (2022).
- [16] S. Karube, *et al.*, Observation of spin-splitter torque in collinear antiferromagnetic RuO₂. *Phys. Rev. Lett.* **129**, 137201 (2022).
- [17] Y. Guo, *et al.*, Direct and inverse spin splitting effects in altermagnetic RuO₂. *Adv. Sci.* **11**, 2400967 (2024).
- [18] H. Bai, *et al.*, Efficient spin-to-charge conversion via altermagnetic spin splitting effect in antiferromagnet RuO₂. *Phys. Rev. Lett.* **130**, 216701 (2023).
- [19] T. Berlijn, *et al.*, Itinerant antiferromagnetism in RuO₂. *Phys. Rev. Lett.* **118**, 077201 (2017).
- [20] Z. H. Zhu, *et al.*, Anomalous antiferromagnetism in metallic RuO₂ determined by resonant x-ray scattering. *Phys. Rev. Lett.* **122**, 017202 (2019).
- [21] Z. L. Lin, *et al.*, Observation of giant spin splitting and *d*-wave spin texture in room temperature altermagnet RuO₂. arXiv:2402.04995 (2024).
- [22] A. Smolyanyuk, I. I. Mazin, L. Garcia-Gassull, and R. Valentí, Fragility of the magnetic order in the prototypical altermagnet RuO₂. *Phys. Rev. B* **109**, 134424 (2024).
- [23] M. Hiraishi, *et al.*, Nonmagnetic ground state in RuO₂ revealed by Muon spin rotation. *Phys. Rev. Lett.* **132**, 166702 (2024).
- [24] O. Fedchenko, *et al.*, Observation of time-reversal symmetry breaking in the band structure of altermagnetic RuO₂. *Sci. Adv.* **10**, eadj4883 (2024).

- [25] X. Feng, *et al.*, Incommensurate spin density wave in antiferromagnetic RuO₂ evinced by abnormal spin splitting torque. *Phys. Rev. Lett.* **132**, 086701 (2024).
- [26] S. G. Jeong, *et al.*, Altermagnetic polar metallic phase in ultra-thin epitaxially-strained RuO₂ films. arXiv:2405.05838 (2024).
- [27] M. Weber, *et al.*, All optical excitation of spin polarization in *d*-wave altermagnets. arXiv:2408.05187 (2024).
- [28] H. Nakayama, *et al.*, Spin Hall magnetoresistance Induced by a nonequilibrium proximity effect. *Phys. Rev. Lett.* **110**, 206601 (2013).
- [29] J. Kim, P. Sheng, S. Takahashi, S. Mitani, and M. Hayashi, Spin Hall magnetoresistance in metallic bilayers. *Phys. Rev. Lett.* **116**, 097201 (2016).
- [30] H. Nakayama, *et al.*, Rashba-Edelstein magnetoresistance in metallic heterostructures. *Phys. Rev. Lett.* **117**, 116602 (2016).
- [31] Z. Q. Wang, *et al.*, Inverse spin Hall effect dominated spin-charge conversion in (101) and (110)-oriented RuO₂ films. *Phys. Rev. Lett.* **133**, 046701 (2024).
- [32] C.-T. Liao, Y.-C. Wang, Y.-C. Tien, S.-Y. Huang, and D. Qu, Separation of inverse altermagnetic spin-splitting effect from inverse spin Hall effect in RuO₂. *Phys. Rev. Lett.* **133**, 056701 (2024).
- [33] See Supplemental Material for methods, additional data and discussions, which includes refs. [34–44].
- [34] G. Kresse, and D. Joubert, From ultrasoft pseudopotentials to the projector augmented-wave method. *Phys. Rev. B* **59**, 1758–1775 (1999).
- [35] G. Kresse, and J. Furthmüller, Efficient iterative schemes for ab initio total-energy calculations using a plane-wave basis set. *Phys. Rev. B* **54**, 11169–11186 (1996).
- [36] J. P. Perdew, K. Burke, and M. Ernzerhof, Generalized gradient approximation made simple. *Phys. Rev. Lett.* **77**, 3865–3868 (1996).
- [37] V. I. Anisimov, J. Zaanen, and O. K. Andersen, Band theory and Mott insulators: Hubbard U instead of Stoner I. *Phys. Rev. B* **44**, 943–954 (1991).

- [38] S. L. Dudarev, G. A. Botton, S. Y. Savrasov, C. J. Humphreys, and A. P. Sutton, Electron-energy-loss spectra and the structural stability of nickel oxide: An LSDA+U study. *Phys. Rev. B* **57**, 1505–1509 (1998).
- [39] N. Marzari, A. A. Mostofi, J. R. Yates, I. Souza, and D. Vanderbilt, Maximally localized Wannier functions: Theory and applications. *Rev. Mod. Phys.* **84**, 1419–1475 (2012).
- [40] A. A. Mostofi *et al.*, An updated version of wannier90: A tool for obtaining maximally-localised Wannier functions. *Comput. Phys. Commun.* **185**, 2309–2310 (2014).
- [41] J. Železný, Y. Zhang, C. Felser, and B. Yan, Spin-polarized current in noncollinear antiferromagnets. *Phys. Rev. Lett.* **119**, 187204 (2017).
- [42] J. Sinova, S. O. Valenzuela, J. Wunderlich, C. H. Back, and T. Jungwirth, Spin Hall effects. *Rev. Mod. Phys.* **87**, 1213–1260 (2015).
- [43] J. R. Yates, X. Wang, D. Vanderbilt, and I. Souza, Spectral and Fermi surface properties from Wannier interpolation. *Phys. Rev. B* **75**, 195121 (2007).
- [44] V. Laukhin *et al.*, Electric-field control of exchange bias in multiferroic epitaxial heterostructures. *Phys. Rev. Lett.* **97**, 227201 (2006).
- [45] A. Nomura, T. Tashiro, H. Nakayama, and K. Ando, Temperature dependence of inverse Rashba-Edelstein effect at metallic interface. *Appl. Phys. Lett.* **106**, 212403 (2015).
- [46] Y. Ou, C.-F. Pai, S. Shi, D. C. Ralph, and R. A. Buhrman, Origin of fieldlike spin-orbit torques in heavy metal/ferromagnet/oxide thin film heterostructures. *Phys. Rev. B* **94**, 140414 (2016).
- [47] H. Nakayama, *et al.*, Temperature dependence of Rashba-Edelstein magnetoresistance in Bi/Ag/CoFeB trilayer structures. *Appl. Phys. Lett.* **110**, 222406 (2017).
- [48] M. Kawaguchi, D. Towa, Y.-C. Lau, S. Takahashi, and M. Hayashi, Anomalous

- spin Hall magnetoresistance in Pt/Co bilayers. *Appl. Phys. Lett.* **112**, 202405 (2018).
- [49] W. Gil, D. Görlitz, M. Horisberger, and J. Kötzler, Magnetoresistance anisotropy of polycrystalline cobalt films: Geometrical-size and domain effects. *Phys. Rev. B* **72**, 134401 (2005).
- [50] P. Qin, *et al.*, Room-temperature magnetoresistance in an all-antiferromagnetic tunnel junction. *Nature* **613**, 485–489 (2023).
- [51] X. Chen, *et al.*, Octupole-driven magnetoresistance in an antiferromagnetic tunnel junction. *Nature* **613**, 490–495 (2023).
- [52] D.-F. Shao, and E. Y. Tsymbal, Antiferromagnetic tunnel junctions for spintronics. *npj Spintronics* **2**, 13 (2024).
- [53] D.-F. Shao, S.-H. Zhang, G. Gurung, W. Yang, and E. Y. Tsymbal, Nonlinear anomalous Hall effect for Néel vector detection. *Phys. Rev. Lett.* **124**, 067203 (2020).
- [54] C. Wang, Y. Gao, and D. Xiao, Intrinsic nonlinear Hall effect in antiferromagnetic tetragonal CuMnAs. *Phys. Rev. Lett.* **127**, 277201 (2021).
- [55] S. Hayami, Y. Yanagi, and H. Kusunose, Momentum-dependent spin splitting by collinear antiferromagnetic ordering. *J. Phys. Soc. Jpn.* **88**, 123702 (2019).
- [56] L.-D. Yuan, Z. Wang, J.-W. Luo, E. I. Rashba, and A. Zunger, Giant momentum-dependent spin splitting in centrosymmetric low- Z antiferromagnets. *Phys. Rev. B* **102**, 014422 (2020).
- [57] Y.-P. Zhu, *et al.*, Observation of plaid-like spin splitting in a noncoplanar antiferromagnet. *Nature* **626**, 523–528 (2024).
- [58] P.-X. Qin, *et al.*, Noncollinear spintronics and electric-field control: a review. *Rare Metals* **39**, 95-112 (2020).
- [59] H. Chen, *et al.*, Emerging antiferromagnets for spintronics. *Adv. Mater.* **36**, 2310379 (2024).
- [60] H. Yan, X. Zhou, P. Qin, and Z. Liu, Review on spin-split antiferromagnetic

spintronics. *Appl. Phys. Lett.* **124**, 030503 (2024).

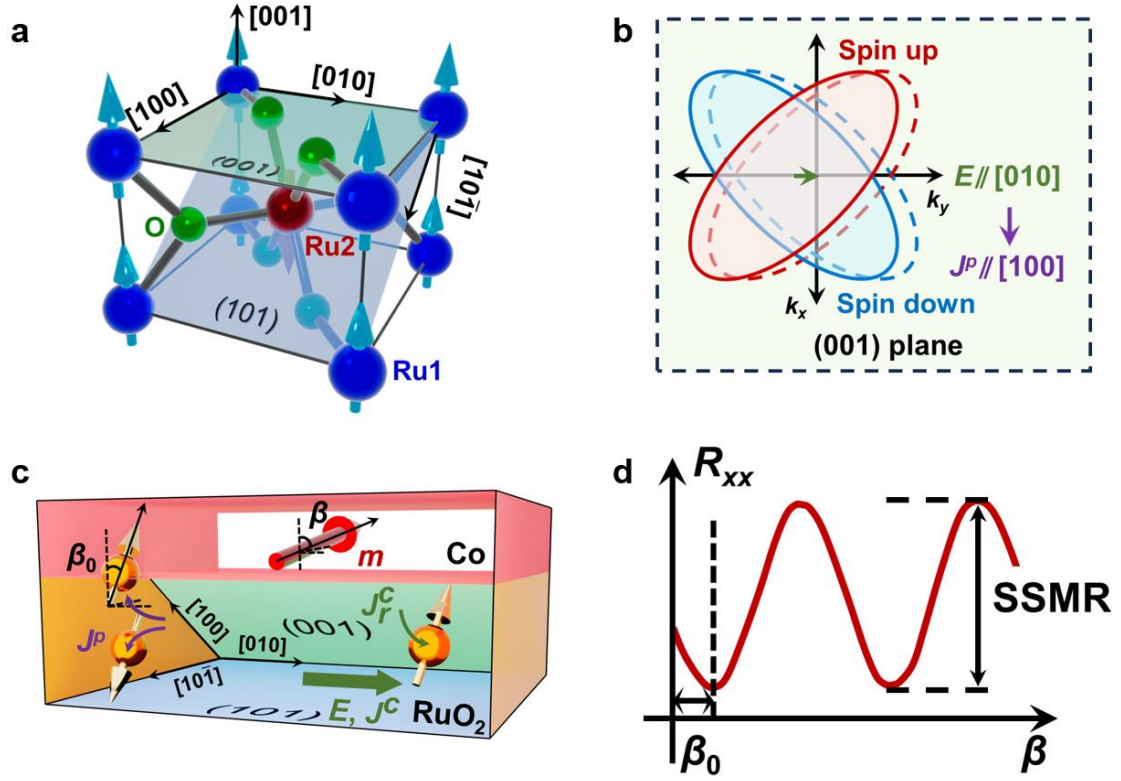


FIG. 1. (a) Crystal structure of RuO_2 . The green and blue shadowed regions are the (001) and (101) plane, respectively. The dark blue and dark red balls represent the Ru atoms with opposite magnetic moment as indicated by the light blue and light red arrows, respectively. The green balls denote the O atoms. (b) Schematic of the spin-splitting effect (SSE). An electric field \mathbf{E} applied along [010] shifts the anisotropic spin-split Fermi contours (the red and blue shadowed ellipses), resulting in a net nonrelativistic spin current \mathbf{J}^p along [100] with polarization \mathbf{p} . \mathbf{p} is parallel to the Néel vector of RuO_2 . (c) Schematic of the SSMR in a (101)-oriented RuO_2/Co bilayer. An applied \mathbf{E} (charge current \mathbf{J}^c) along [010] engenders an out-of-plane \mathbf{J}^p that is illustrated by the movement of electrons (orange balls) with their spin moment (yellow arrows) parallel to \mathbf{p} . β_0 is the out-of-plane tilting angle of \mathbf{p} . The \mathbf{J}^p is reflected by the RuO_2/Co interface, leading to a longitudinal charge current \mathbf{J}_r^c that lowers the resistance of the heterostructure. The magnitude of \mathbf{J}_r^c is modulated by the out-of-plane tilting angle β of the magnetization unit vector \mathbf{m} of the Co layer in a plane perpendicular to \mathbf{E} . (d) Envisaged longitudinal resistance R_{xx} as a function of β in the SSMR.

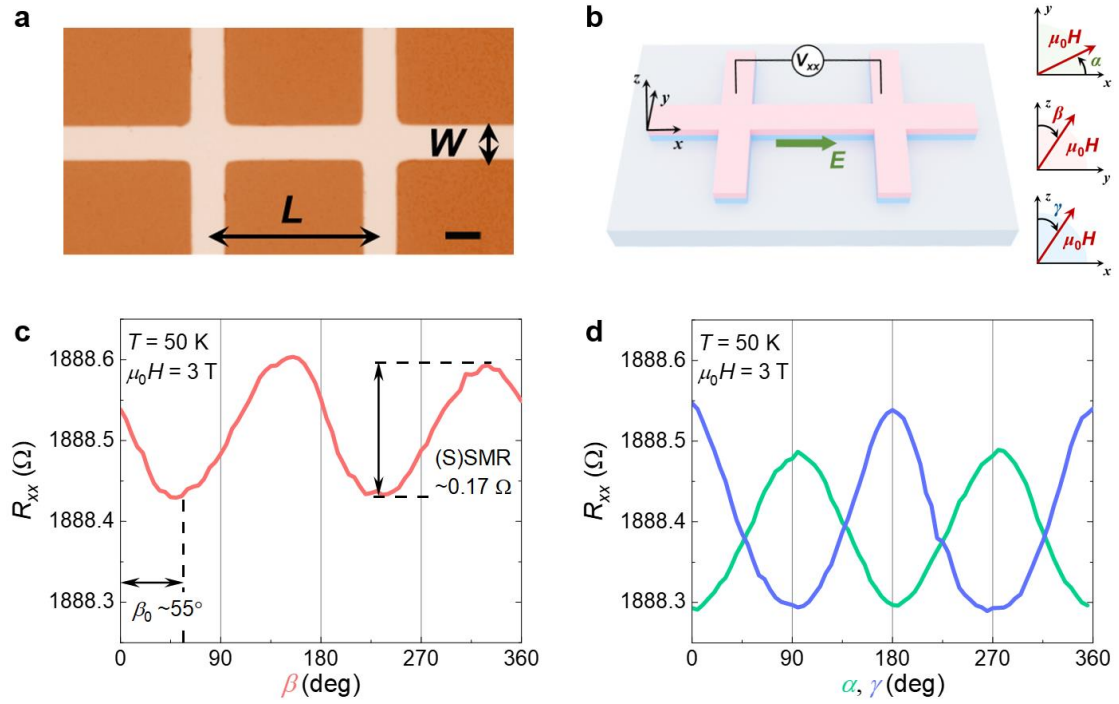


FIG. 2. (a) Optical image of a typical Hall bar device with width W and length L and $L/W \sim 5$. The scale bar is $3 \mu\text{m}$. (b) Schematics of the coordinate system and the rotation angle α , β , and γ of the magnetic field $\mu_0 H$ in our measurements. The longitudinal voltage V_{xx} is detected with E applied along the x axis. (c,d) R_{xx} as a function of α , β , and γ at temperature $T = 50$ K and $\mu_0 H = 3$ T. The β_0 and the (S)SMR can be extracted from the $R_{xx}(\beta)$ curve.

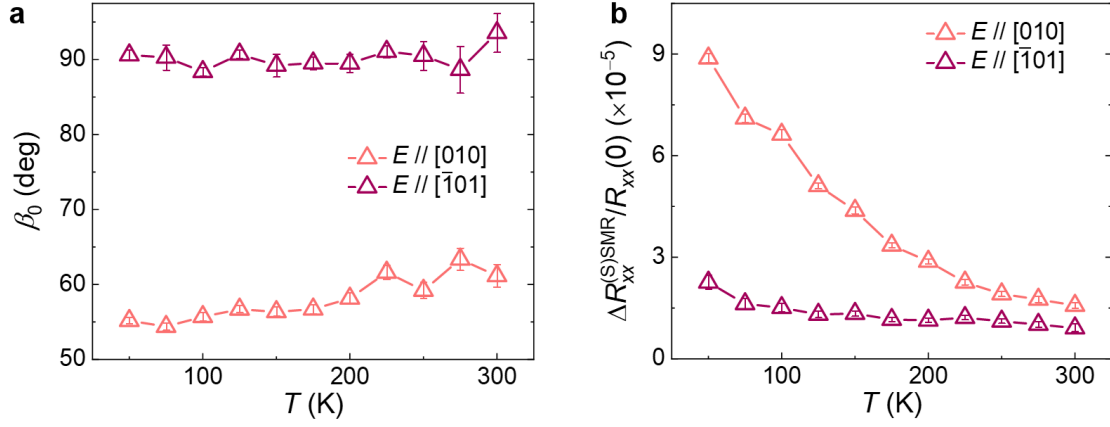


FIG. 3. (a) β_0 and (b) (S)SMR ratio $\Delta R_{xx}^{(S)SMR}/R_{xx}(0)$ measured along two orthogonal in-plane directions as a function of T for the (101)-RuO₂(3 nm)/Co(2.5 nm) sample. $\Delta R_{xx}^{(S)SMR}$ is the (S)SMR effect and $R_{xx}(0)$ is the longitudinal resistance at $\beta = 0^\circ$. The details for the calculation of β_0 , $\Delta R_{xx}^{(S)SMR}/R_{xx}(0)$, and the error bars can be found in Supplemental Note 1 [33].

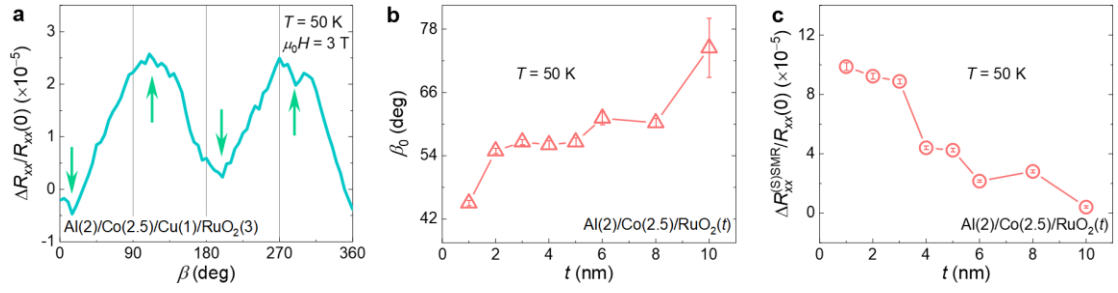


FIG. 4. (a) (S)SMR of a (101)-RuO₂(3 nm)/Cu(1 nm)/Co(2.5 nm) control sample. ΔR_{xx} is calculated as $R_{xx}(\beta) - R_{xx}(0)$. The light green arrows highlight the β where the extrema of $\Delta R_{xx}/R_{xx}(0)$ occur. (b) β_0 and (c) $\Delta R_{xx}^{(S)SMR}/R_{xx}(0)$ as a function of RuO₂ thickness t measured at 50 K in a series of RuO₂(t)/Co(2.5 nm) heterostructures. The numbers in the brackets denote the thickness of the corresponding layer in units of nm.

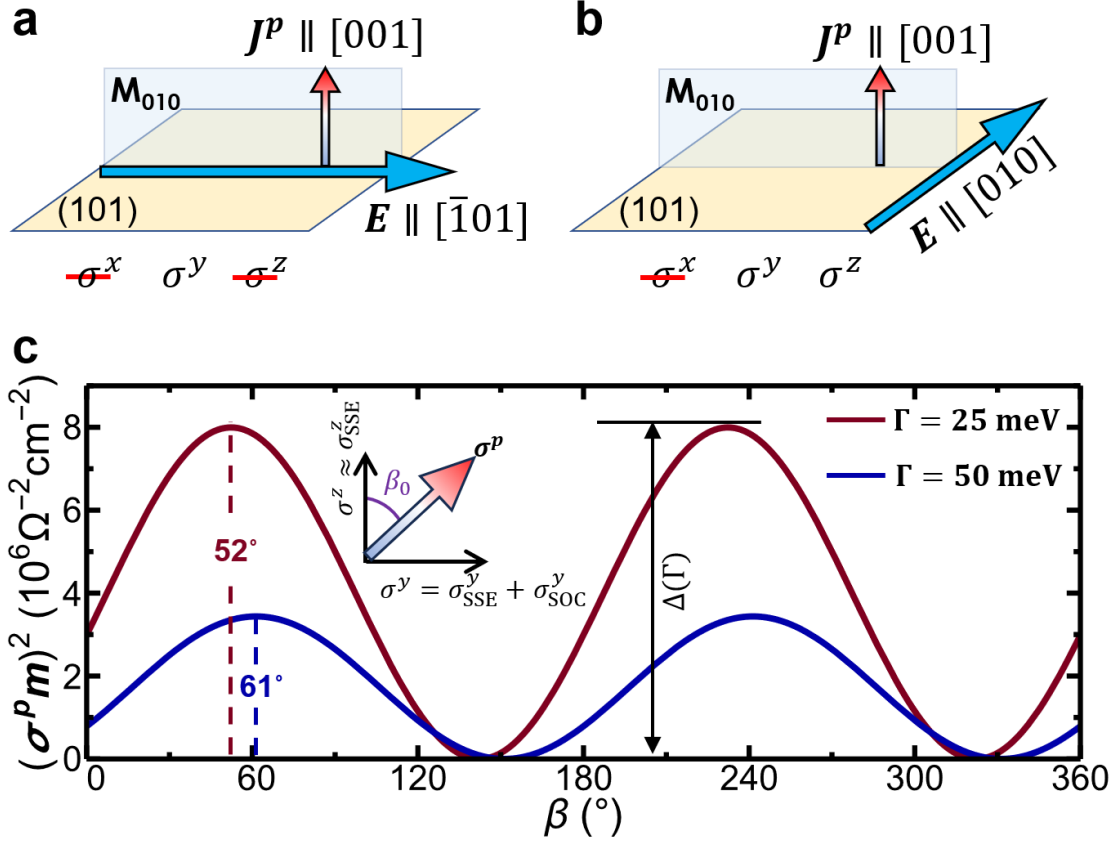


FIG. 5. (a,b) Schematic illustration of the J^p induced by E in (101)-RuO₂ thin films. An electric field E generates an out-of-plane spin current J^p as $J^p = \sigma^p E$, where $\sigma^p = (\sigma^x, \sigma^y, \sigma^z)$ is the spin conductivity and p is the spin polarization direction. For $E // [\bar{1}01]$, only the spin conductivity component σ^y is allowed by the glide mirror plane M_{010} . For $E // [010]$, the spin conductivity component σ^x is forbidden by M_{010} . (c) Calculated β dependence of $(\sigma^p m)^2$ of RuO₂ (101) for $E // [010]$, where the unit vector of the magnetization of Co $m = (0, \sin\beta, \cos\beta)$. In RuO₂ (101), we expect $\sigma^p = (0, \sigma_{\text{SSE}}^y + \sigma_{\text{SOC}}^y, \sigma_{\text{SSE}}^z)$, where the spin-orbit coupling (SOC) induced spin conductivity σ_{SOC}^y is fixed to $1000 (\Omega \text{cm})^{-1}$, and the SSE induced spin conductivity $\sigma_{\text{SSE}}^{y(z)}$ is calculated with the energy broadening Γ of 25 meV and 50 meV. We define the difference between the maximum and minimum $(\sigma^p m)^2$ as $\Delta\Gamma$. The vertical dashed lines denote β_0 .